17th international heat pipe conference
kanpur, india
October 14 - 17, 2013

EVALUATION OF THE VAPOR THERMODYNAMIC STATE IN PHP

P. Gully[1], F. Bonnet[1], V. Nikolayev[2], N. Luchier[1], T.Q. Tran[1]

[1]CEA-INAC/SBT, UMR_E 9004 CEA-UJF Grenoble, 38054 Cedex 9, France
[2] IRAMIS/SPEC, URA CNRS 2464, CEA Saclay, 91191 Gif-sur-Yvette Cedex, France
Phone: (+33)-(0)4 38 78 32 40, Fax: (+33)-(0)4 38 78 51 71

ABSTRACT Pulsating Heat Pipe (PHP) is a recently invented kind of thermal link of high thermal performance. The heat is transferred due to self-sustained oscillations of vapor bubbles and liquid plugs in a unique capillary tube which links the hot and cold sources in several turns or branches. Increasingly strong efforts are devoted to PHP simulation models which need to be experimentally assessed. Recent models show the importance of the thermodynamic state of the vapor bulk. Indeed it may deviate from the saturation conditions due to vapor transient compression/expansion. This study aims at measuring and calculating the vapor state in a horizontal single branch PHP which allows generating oscillations of a liquid meniscus in a capillary tube with one open end, at which the pressure is imposed. The experimental setup uses oxygen at cryogenic temperatures which reduces as much as possible the radiation losses of both sensors (microscopic thermocouple) used for the direct vapor temperature measurement and of the whole PHP. We present here the simultaneous experimental measurements of the vapor pressure and temperature. The data are compared to the theoretical modeling obtained within the film evaporation/condensation model of PHP [Das et al., 2010]. The model is extended to account for the thermal gradient along and across the tube walls formed because of the poor heat conductivity of its material. The vapor is found superheated, which demonstrates the relevance of the model. The vapor temperature oscillates around the evaporator temperature. The heat transfer between the vapor and the dry evaporator wall explains this result. The corresponding heat transfer coefficient is calculated using DNS. The comparison shows an agreement between the experiment and the model.

KEY WORDS: pulsating heat pipe, vapor temperature measurement.

1. INTRODUCTION

Heat transfer is a crucial problem in many industrial applications where the cold source cannot be located close to the hot source. Thermal links between them must be used; the heat pipes are attractive solutions with low thermal resistance and mass. Among them, the pulsating heat pipe (PHP) is a recent [Akashi, 1993] and promising candidate. It consists of a tube, bent in many turns and filled with a two-phase fluid. The tube diameter must be small enough to ensure the formation of a pattern of vapor bubbles and liquid plugs inside the tube [Khandekar et al., 2010]. The diameter is generally considered to be lower than the capillary length of the fluid. Under a certain temperature difference between the two ends of the PHP the pattern of bubbles and plugs start to move in self-sustained oscillations. The heat transfer mainly comes from phase change (evaporation and condensation), but a part is also transported by the liquid plugs. Such a heat transfer process leads to high thermal performances [Maydanik et al., 2009]. The simplicity and the high performance of the PHP make it a particularly promising thermal link. Nevertheless, industrial applications of PHP are made complicated by the non-equilibrium nature of the mechanism responsible for the oscillations, which are not yet well controlled. Many experiments have been performed. Most of them are reported by Zhang et al. [2002] and no simple understanding of the mechanisms has emerged. A complete model describing all local mechanisms involved in the PHP is therefore needed to be developed.

Das et al. [2010] proposed a thermo hydraulic model describing the self-sustained oscillations in a single branch PHP based on the film evaporation-condensation. Nikolayev [2011] applied it to build a simulation code aiming

*Corresponding Author: philippe.gully@cea.fr

at calculating the whole thermo hydraulic behavior of a PHP. The startup of oscillations has been studied recently [Nikolayev, 2013] within this model. It is based on an assumption that strong temperature gradients exist inside the vapor phase. While the gas-liquid interface is at saturation temperature, the vapor bulk temperature may deviate from it. Vapor pressure variation is given by the ideal gas law rather than by the saturation curve. The vapor may thus be superheated or undercooled; the nucleation barrier is assumed to be high enough to prevent the volume condensation in the latter case.

In this paper we present and discuss experimental results on the thermodynamic state of the vapor bubble of a single branch PHP, where simultaneous and fast pressure and temperature measurements in the vapor phase are performed. The experimental data are compared to the numerical results obtained within the film evaporation-condensation model upgraded to account for the experimental conditions.

2. EXPERIMENTAL SET UP

Generally, it is quite difficult to measure the gas temperature inside a hot container. The thermocouple sensor usually used for this purpose is submitted to parasite heat fluxes, the strongest of which is the radiative heat flux from the hot container walls proportional to T^4. At the same time, the convective heat exchange of the thermocouple with the gas is weak which means that the thermocouple in the water PHP at atmospheric pressure would register basically the wall temperature. A conventional way of overcoming this problem is the thermocouple screening. However for the PHP applications this solution is almost impossible because of the small tube diameter. The gas temperature measurement has thus been performed at cryogenic temperature, where the radiative heat exchange is negligible.

The experimental set-up is presented in Figure 1. It features a single branch PHP with a single liquid plug and a single vapor bubble. One end is blind and another is connected to a constant pressure reservoir. The meniscus oscillations can be sustained by the evaporation/condensation process. The PHP consists of a single stainless steel horizontal tube (d =2 mm inner and d_o =3 mm outer diameter, roughness less than 1µm). The tube is brazed into a 150 mm copper evaporator and into a 150 mm copper condenser.

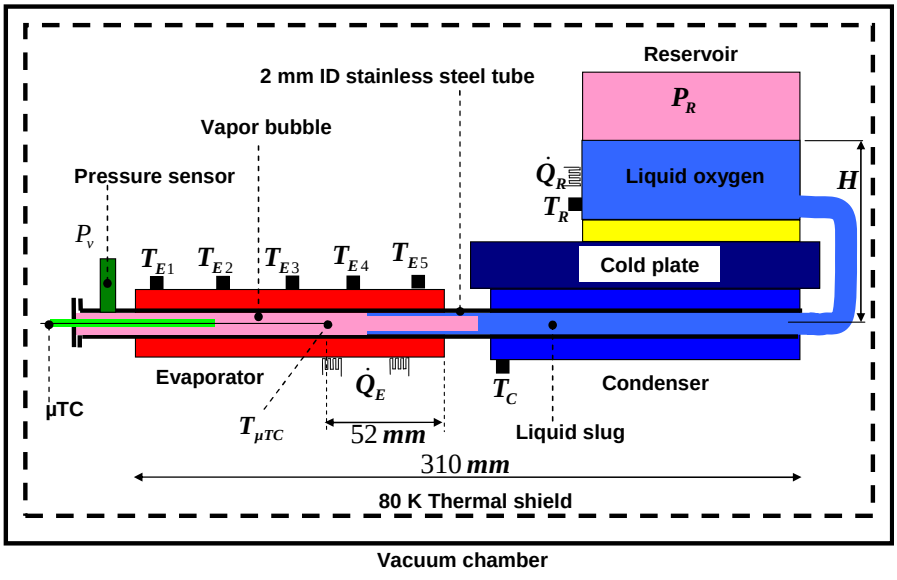

FIG. 1: Experimental set up with instrumentation.

Two local electrical heaters allow delivering a total heating power $\dot{Q}_E$ to the evaporator on its first third. The condenser is anchored to the isothermal cold plate of the cold source. A 10 mm adiabatic section separates the evaporator from the condenser. The experimental apparatus operates at cryogenic temperatures (60 K – 70 K) using oxygen as working fluid. A thermal shield cooled by liquid nitrogen protects properly the PHP against

external parasite heat loads. Such cryogenic conditions allow knowing precisely the heat power transferred in the evaporator and the condenser. The cold source is provided by a Gifford McMahon cryocooler. The condenser temperature T_C can be very easily adjusted using a PID regulation. The reservoir temperature T_R can be adjusted using electrical heating $\dot{Q}_R$. Since the reservoir is partially filled by liquid, T_R fixes the reservoir pressure $P_R = P_{SAT}(T_R)$. Both the condenser and the evaporator are equipped with thermal sensors. They are all of the Pt100 type except T_{E3} which is a calibrated Cernox Lakeshore sensor. The reservoir pressure is measured at room temperature using a classical pressure transducer. The saturation reservoir temperature taking into account the liquid level is given by the expression $T_{r,SAT} = T_{SAT}(P_R + \rho_L g H)$, where ρ_L, g and H are respectively the liquid density, the gravity acceleration and the reservoir liquid level. All mentioned temperatures are measured or calculated within ±0.2 K.

The blind end of the evaporator, always in pure vapor phase, is equipped with a fast cold pressure miniature sensor P_v (Kulite ref. CT-190). Owing to the in situ calibration, this sensor allows the determination of the vapor bubble saturation temperature $T_{SAT}(P_v)$ within ±0.2 K.

The vapor temperature is measured using an unsheathed micro thermocouple (µTC). Its spherical sensitive end 30 µm in diameter is located inside the evaporator. Details on the µTC are given in Figure 2 and Figure 3. Assuming negligible effect of the two 13 µm wires, the time constant of µTC is expressed as $\tau_{\mu TC} = \frac{1}{h}\left(\frac{\rho V C}{A}\right)_{\mu TC}$, where h, ρ, V, C and A are respectively the heat transfer coefficient between the µTC sensitive end and the vapor, the density, the volume, the specific heat and the heat transfer surface of the spherical sensitive end.

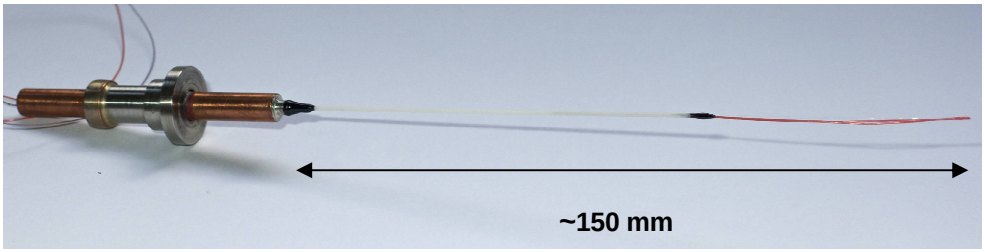

FIG. 2: Photography of the µTC.

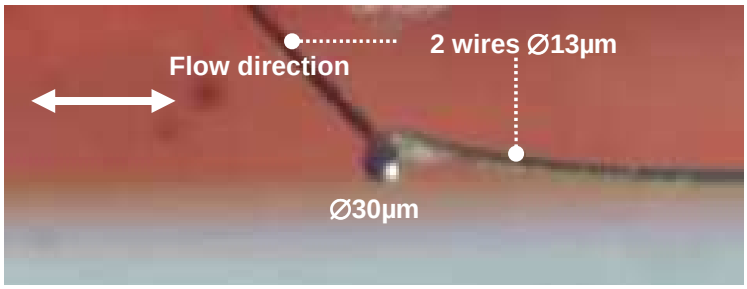

FIG. 3: Sensitive end of the µTC.

The vapor flows at a very low Reynolds number around the spherical end. The Nusselt number is therefore constant (Nu=2) and conduction through the vapor is the main heat transfer channel. The heat transfer coefficient h~300 $Wm^{-2}K$ is constant. The small size of µTC and the small specific heat that occurs at cryogenic temperatures lead to a small time constant of $\tau_{\mu TC}$~30 ms compatible with the investigated oscillation frequency range (f ~1-2 Hz).

Note that the operation at cryogenic temperatures makes the µTC insensitive to the effect of thermal radiation from the tube internal surface. Indeed, the radiation heat transfer coefficient h_{RAD} between the µTC and the evaporator wall is expressed for small temperature difference $T_E - T_{\mu TC}$ as follows:

$$h_{RAD} = \frac{\dot{Q}_{RAD}}{\left(T_E - T_{\mu TC}\right) A} = \frac{\sigma A\left(T_E^4 - T_{\mu TC}^4\right)}{\left(T_E - T_{\mu TC}\right) A} \approx 4\sigma T_E^3 \sim 0.1 \text{ Wm}^{-2}\text{K}^{-1},$$

where σ=5.670373×10^{-8} W m^{-2}K^{-4} is the Stefan-Boltzmann constant and the emissivity is assumed to be unity for the estimation purpose. At cryogenic temperatures, $h_{RAD} << h$ and is thus negligible.

The µTC is calibrated in situ to check its sensitivity. A global precision of ±0.2 K is achieved using a high precision voltmeter (Keithley 3706).

The temperature range is adjusted to obtain a small oscillation frequency which is proportional to the square root of the pressure [Das et al., 2010]. The use of oxygen in the range 60 K – 70 K allows us getting a very low pressure (about 100 hPa) and 1-2 Hz oscillation frequency may be achieved. This frequency is compatible with the data acquisition system maximum frequency (50 Hz) imposed by the precision requirement for a low analog signal of the µTC. For the assumed harmonic oscillation of the µTC temperature $T_{\mu TC}$, the deviation from its time average with respect to the deviation of the vapor temperature T_v may be estimated with the following expression

$$\left(\frac{T_{\mu TC} - \bar{T}_{\mu TC}}{T_v - \bar{T}_v}\right)_{MAX} \approx \frac{1}{\sqrt{1 + \left(2\pi\tau_{\mu TC} f\right)^2}} \approx 2\%.$$

$T_{\mu TC}$ is thus expected to be within ±0.2 K from the actual T_v which means that the time response of the µTC is adequate for 1-2 Hz frequency. However it might be insufficient if T_v varied faster.

Finally, the parameters governing the thermal behavior of the presented single branch PHP are the condenser temperature T_C, the reservoir pressure P_R (i.e., $T_{r,SAT}$) and the heating power $\dot{Q}_E$ applied to the evaporator.

3. DNS OF THE GAS-WALL EXCHANGE

To evaluate the thermal convection/diffusion vapor heat exchange with the internal tube walls, a direct numerical simulation (DNS) was performed with the ANSYS CFX software.
The vapor is supposed to be a perfect gas situating inside a tube closed at one end and having an oscillating piston at the other end (to model the meniscus). The simulation conditions mimic the above experiment as close as possible. The isothermal boundary conditions at T_E=72.5 K are imposed at the tube walls, while the zero heat flux is imposed at the piston surface and the opposite blind tube end. The oscillation amplitude is adjusted to match the pressure oscillation amplitude observed in the above experiment. The 2D axisymmetric transient problem of heat diffusion and convection is solved in the gas.
The calculation shows a laminar axial oscillating flow. The Nusselt number (Figure 4) is slightly larger (Nu_v=6) than the value of 4, well-known for the steady state laminar flow.

4. PHP SIMULATION

The film evaporation-condensation model [Das et al., 2010] was used to model the single-branch PHP of Figure 1. Since the experimental PHP may show important temperature gradients in the stainless steel tube which is a

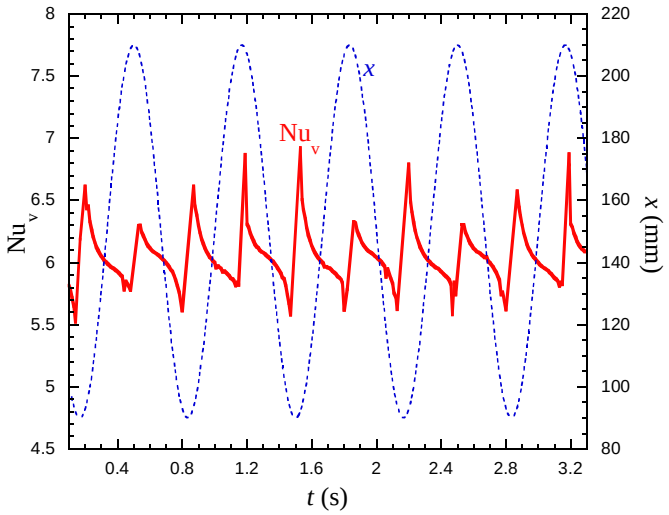

FIG. 4: The Nusselt number Nu_v obtained with DNS for imposed oscillations of the piston (coordinate of the piston surface: x; x=0 at the blind tube end).

poor heat conductor under cryogenic temperatures, the model was extended by considering the heat diffusion in the PHP tube (evaporator and adiabatic sections, cf. Figure 5) coupled with the fluid description. Instead of the isothermal evaporator and adiabatic section, the fixed average heat flux was imposed.

The simulated PHP tube consists of two layers made of stainless steel and copper, respectively. For the simulation purposes, the copper layer was assumed to be a cylinder (Figure 5) with the effective external diameter d_e =7 mm that provides the same cross-section copper area S_{Cu} as in the experiment. The governing equations of stainless steel temperature T_s and copper temperature T_{Cu} are:

$$\frac{\partial T_s}{\partial t} = D_s \frac{\partial^2 T_s}{\partial x^2} + \frac{j_s}{\rho_s C_s}, \tag{1}$$

$$\frac{\partial T_{Cu}}{\partial t} = D_{Cu} \frac{\partial^2 T_{Cu}}{\partial x^2} + \frac{j_{Cu}}{\rho_{Cu} C_{Cu}}, \tag{2}$$

with the equivalent volume heat fluxes

$$j_s = \pi \frac{q_{fluid} d + q_{Cu} d_o}{S_s}, \qquad j_{Cu} = \pi \frac{q_h d_e - q_{Cu} d_o}{S_{Cu}}.$$

The variables that enter these expressions are detailed below (cf. also Figure 5). The copper shell is assumed to be isothermal in its cross-section. The temperature T_s corresponds to the interface fluid-stainless steel. The temperature drop inside the stainless steel in the radial direction is accounted for with a thermal resistance $R_s = \frac{d_o}{2k_s} \ln \frac{d_o}{d}$. The surface heat flux at the stainless steel-copper interface is $q_{Cu} = \frac{T_{Cu} - T_s}{R_s}$. The heat flux $q_{fluid} = h_{fluid}(x)\left[T_{fluid}(x) - T_s\right]$ at the fluid-stainless steel interface involves the heat exchange coefficient

$$h_{fluid}(x) = \begin{cases} k_v \mathrm{Nu}_v / d, & \text{if } x \in \text{vapor bubble}, \\ k_l \gamma / \delta, & \text{if } x \in \text{liquid film}, \\ k_l \mathrm{Nu}_l / d, & \text{if } x \in \text{liquid plug}. \end{cases}$$

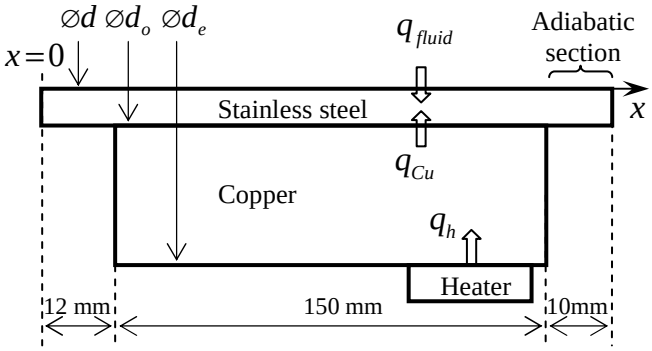

FIG. 5: Representation in simulation of the PHP tube cross-section (lower half of the evaporator and adiabatic sections). The zero heat flux conditions are imposed at all external surfaces of the structure except the adiabatic section (rightmost) end where the isothermal condition $T_s = T_C$ is enforced.

It is assumed that $T_{fluid}(x) = T_{SAT}(P_v)$ if x belongs to the liquid film and $T_{fluid}(x) = T_C$ if x belongs to the liquid plug. The zero heat flux boundary conditions are imposed for T_s from the heater is $q_h = \dfrac{\dot{Q}_E}{\pi d_e l_h}$ where l_h =50 mm is the effective length of evaporator covered by the electric heater. The remaining equations of the model coincide with those of Das et al. [2010]. Unlike the Das et al. model, the end x_E of the film evaporation area is not fixed at the boundary between the evaporator and adiabatic sections. This point is instead defined by the equation $T_s(x_E) = T_{SAT}(P_v)$ and moves periodically between the evaporator and adiabatic sections. The finite volume numerical method is used to solve Eqs. (1-2). The discretization mesh is nearly equidistant, with the element length of 1 mm.

5. RESULTS AND DISCUSSION

5.1 Experimental results

A typical experimental result is presented in Figure 6. For this test the condenser temperature, the reservoir temperature and the heat power applied on the evaporator are respectively 66.2 K, 70 K and 1.5 W. The saturation temperature $T_{SAT}(P_v)$ of the vapor bubble is calculated from the measured vapor pressure P_v which oscillates between 30 and 80 hPa. The oscillation frequency is 1.5 Hz. The amplitude of oscillations of the saturation temperature is constant (1.5 K). The saturation temperature oscillates around the temperature $T_{r,SAT}$, imposed by the reservoir. The vapor temperature $T_{\mu TC}$ is found to be always greater than the saturation temperature, showing a superheated state. The vapor temperature fluctuates (±0.5 K) around the mean evaporator temperature defined as $T_E = 1/5(T_{E1} + T_{E2} + T_{E3} + T_{E4} + T_{E5})$ =72.7K. The heat transfer between the vapor and the dry hot wall of the evaporator during the meniscus receding can explain this result. We verified that the introduction of the µTC does not influence the pressure variation and the thermal regime for this measurement, in which the results with and without µTC inside the PHP, are almost identical. In some cases, the µTC was apparently reached by the liquid plug and dried which influenced the oscillation regime.

5.2 Results of the model

We used Nu_v=6 obtained in the above DNS, δ =16.5 µm the film thickness (assumed to be constant), γ =1.7 as a coefficient accounting for the inhomogeneous film thickness, the equivalent liquid laminar flow viscous friction length (1.8 m) and the liquid plug "inertial" length (0.4 m) that controls the oscillation frequency. A recent study [Khandekar, 2013] shows that Nu_l may be one order of value larger that of the laminar liquid flow. We used Nu_l =20. As expected, the temperature gradient in the stainless steel tube is not negligible; the

temperature of its blind end is close to the average copper block temperature T_E while the adiabatic section end is (imposed to be) at the temperature T_C.

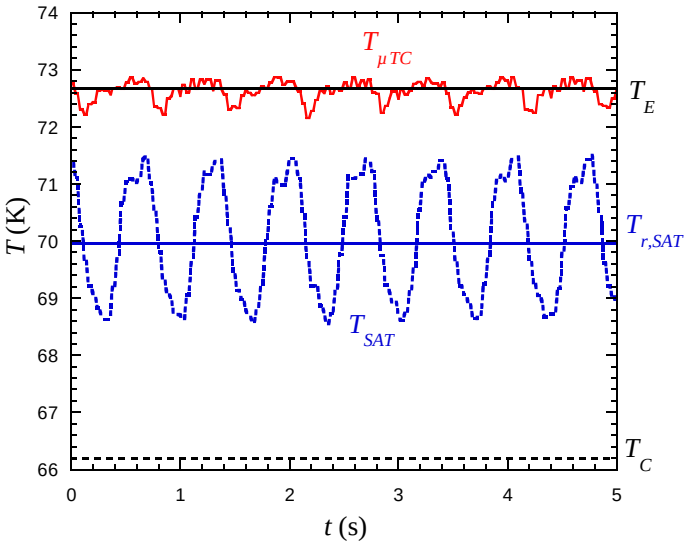

FIG. 6: Experimental results.

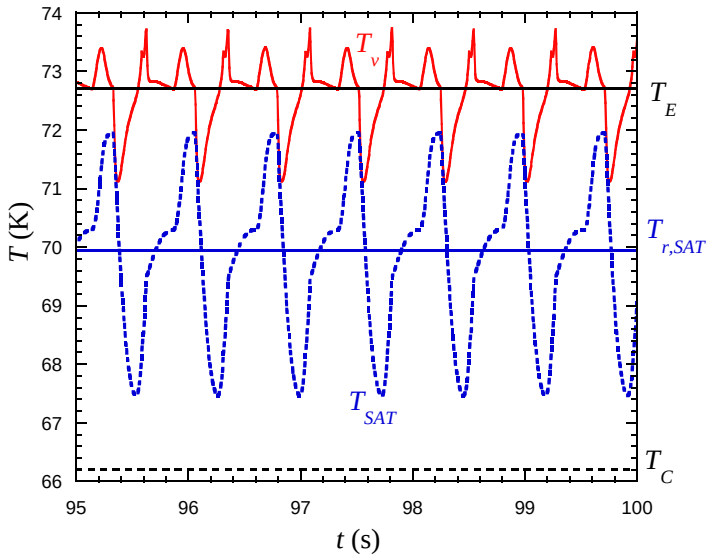

FIG. 7: Simulation results for $\dot{Q}_E$ =1.5W.

Due to the appropriate choice of the simulation parameters discussed above, the oscillation frequency and the evaporator temperature are the same as in the experiment.

Several conclusions may be drawn from the comparison of Figures 6 and 7. The shape of the curves is similar. One may identify a "shoulder" and a peak at which T_{SAT} achieves its maximum. Immediately after attaining this maximum, T_v starts to drop sharply together with the vapor mass because the vapor condensation on the portion of film situating in the condenser overcomes the evaporation of the film part situating in the evaporator. The T_v minimum occurs earlier than that of the pressure: as soon as the meniscus recedes deep enough into the condenser, the vapor mass drops so quickly that its temperature rises to match the weakly changing P_vV_v product according to the ideal gas equation of state. A very important feature reproduced well by the simulation is the average T_v value that corresponds in both cases to T_E. This phenomenon appears because of the heat exchange of the vapor with the dry solid described by the Nu_v coefficient discussed above. While the qualitative features

are reproduced well by the simulation, the simulated oscillation amplitudes are somewhat larger than their experimental counterparts. Since the extrema of the simulated curves are quite sharp (cf. Figure 7), such a discrepancy may be explained by an insufficient frequency response of the measurement sensors.

6. CONCLUSION

This result clearly demonstrates the relevance of the film evaporation/condensation model which assumes that the vapor bulk temperature may be larger than the saturation temperature. The experiment shows that the vapor may reach a temperature even higher than the hot wall temperature. Such a phenomenon is known to be possible transiently in two phase compressible fluids [Wunenburger et al., 2000].

ACKNOWLEDGMENTS

The authors are thankful to David Garcia, Julien Inigo, and Laurent Clerc of INAC/SBT for their help with manufacturing and testing the PHP. The financial support of ANR in the framework of the project AARDECO ANR-12-VPTT-005-02 and of PSA Peugeot-Citroën is acknowledged.

NOMENCLATURE

A	surface area	(m^2)	x	coordinate or plug position	(m)
C	specific heat	(J/kg/K))	γ	liquid film shape factor	(-)
d	diameter	(m)	δ	liquid film thickness	(m)
D	thermal diffusivity	(m^2/s)	ρ	density	(kg/m^3)
f	frequency	(Hz)	σ	Stefan-Boltzmann constant	($W.m^{-2}.K^{-4}$)
H	level in the reservoir	(m)	τ	time constant	(s)
h	heat transfer coefficient	($W/m^2/K$)	C	subscript for condenser	
j	volume heat flux	(W/m^3)	Cu	subscript for copper	
k	heat conductivity	(W/m/K)	E	subscript for evaporator	
l	length	(m)	h	subscript for heater	
Nu	Nusselt number	(-)	e	subscript for external	
P	pressure	(Pa)	l	subscript for liquid	
q	heat flux	(W/m^2)	o	subscript for outer	
$\dot{Q}$	heating power	(W)	r, R	subscript for reservoir	
R	thermal resistance	($K.m^2/W$)	s	subscript for stainless steel	
S	cross section area	(m^2)	SAT	subscript for saturation	
T	temperature	(K)	v	subscript for vapor	
$\overline{T}$	time-averaged temperature	(K)			

REFERENCES

1. Akachi, H., “Structure of micro-heat pipe”, US Patent 5219020, (1993).
2. Das, S.P., Nikolayev, V.S., Lefevre, F., Pottier, B., Khandekar, S. & Bonjour, J., ”Thermally induced two-phase oscillating flow inside a capillary tube", Int. J. Heat Mass Transfer, Vol. 53, pp. 3905-3913, (2010).
3. Khandekar, S. 2013, personal communication, see also his presentation at this conference
4. Khandekar, S., Panigrahi, P.K., Lefevre, F. and Bonjour, J., “Local hydrodynamics of flow in a pulsating heat pipe: a review”, Frontiers in Heat Pipes, Vol. 1, 023003, (2010).
5. Maydanik, Y.F., Dmitrin, V.I., Pastukhov, V.G., “Compact cooler for electronics on the basis of a pulsating heat pipe”, Appl. Therm. Eng., 29 (17-18), pp. 3511-3517, (2009).
6. Nikolayev, V.S., “A Dynamic Film Model of the Pulsating Heat Pipe”, J. Heat Transfer, Vol. 133 (8), 081504, (2001).
7. Nikolayev, V.S., “Oscillatory instability of the gas-liquid meniscus in a capillary under the imposed temperature difference”, Int. J. Heat Mass Transfer, Vol. 64, pp. 313 - 321,(2013).
8. Wunenburger, R., Garrabos, Y., Lecoutre-Chabot, C., Beysens, D. & Hegseth, J., “Thermalization of a Two-Phase Fluid in Low Gravity: Heat Transferred from Cold to Hot”, Phys. Rev. Lett, Vol. 84, pp. 4100 - 4103, (2000).
9. Zhang, Y. and Faghri, A., “Advances and unsolved issues in pulsating heat pipes”, Int. J. Heat Mass Transfer 45 (4), pp. 755-764, (2002).